Proceedings of ASME Turbo Expo 2009
ASME Turbo Expo 2009 Gas Turbine Technical Congress and Exposition
June 8-12, 2009, Orlando, Fla, USA

GT2009-60141

CAPTURING THE SHAPE VARIANCE IN GAS TURBINE COMPRESSOR MAPS

Chris Drummond

Institute for Information Technology
National Research Council Canada
Ottawa, Ontario, Canada, K1A 0R6
Email: Chris.Drummond@nrc-cnrc.gc.ca

Craig R. Davison

Institute for Aeronautical Research
National Research Council Canada
Ottawa, Ontario, Canada, K1A 0R6
Email: Craig.Davison@nrc-cnrc.gc.ca

ABSTRACT

The production of accurate compressor maps is an essential, but time consuming, step in gas turbine engine modeling. Insight into how the shape of a map depends on the compressor type, and design point characteristics, should accelerate this exercise. It should also serve as the basis of a more accurate scaling procedure than is currently available. In this paper, we extract information empirically from a collection of maps for different types of compressor. A technique, used in computer vision, generates smooth transformations between maps, producing intermediate ones of the right form. Not only can the total shape change between maps be determined, but also the principal dimensions of that change. We present figures that capture both typical maps of various types and the most significant dimensions of variation between types. We discuss how these are tied to physical processes within the compressors. We then show how this information can be used to accurately scale maps.

1 Introduction

The production of accurate compressor maps is a critical step in gas turbine engine modeling. They are essential in determining the off-design performance of gas turbine engines. In addition, component models based on them can be combined to produce accurate simulations [1], important both in engine design and diagnostics. However, the generation of such maps is both time and resource consuming. Producing a new one typically starts with a map for a similar compressor which is scaled to match the required characteristics at the design point. A commonly used scaling method is to multiply each of its dimensions by a single factor [2]. This may be satisfactory if the compressor is "sufficiently similar", an ill-defined concept. Even when it is sufficiently similar, a considerable amount of fine tuning by an expert will be needed until the map is acceptable.

Insight into how the shape of a map depends on compressor type, and design point characteristics, should accelerate the modeling process. It should also serve as the basis of a more accurate scaling procedure. Although we hope it will aid engine designers to some degree, our main target is the reverse-engineering of compressor maps carried out by other engineers. The approach, in this paper, is built around a technique used in computer vision which generates smooth transformations between shapes. When applied to human faces, this produces intermediate faces which are still clearly human. It seems likely, therefore, that when applied to compressor maps it should produce intermediate maps of the right form. We use these morphological analysis techniques [3] to learn a shape space capturing the common characteristics of a set of existing maps. As the maps themselves are typically very smooth, it makes sense that transformations between them should be smooth. The transformations are based on a thin-plate spline. Intuitively, imagine trying to bend a thin metal plate to capture the differences between maps. It is relatively easy to bend the plate smoothly, much harder to introduce sudden local bending. The amount of bending is captured in a "bending energy" matrix, quantifying the severity of the shape change.

Not only can the total shape change between maps be determined, but also the principal dimensions of that change can

be identified. A technique called spectral decomposition can applied to a matrix representing the full variance in shape of the compressor maps, weighted by the bending energy matrix. This decomposition produces an ordered list of dimensions, capturing the commonalities between maps, the first few of which represent most of the change. We apply this technique to maps that have been collected from the literature. The maps are of all basic types: fans, axial and radial compressors. We study the variance of shape across all types, as well as within each type.

To gain an understanding of the shape variation, we present figures that capture both typical maps of different types and the significant dimensions of variation. We accompany these figures with discussions on how these dimensions are tied to physical processes within the compressors. We expect that many of our observations will be unsurprising to experienced compressor designers. We hope, though, that some observations are novel and that other less experienced engineers, including students, will gain insight from our analysis. We will also show how this information can be used to accurately scale maps.

2 Capturing Shape Variance

In this section, we begin by highlighting the variety of compressors under study. We continue by introducing the matrix algebra needed to warp smoothly from one map to another. We then show how that warp can be decomposed into a small number of dimensions.

2.1 The Range of Maps

Figure 1 shows the design points for 27 compressors whose maps have been collected from the literature [4–25]. These are the same ones as were used in Kurzke and Riegler's [26] paper introducing a new scaling procedure. The y-axis is the pressure ratio across the compressor; the x-axis is the mass flow through it. The axes use a log scale to more easily see the differences between the design points for smaller values. If the series of mass flows falls on the same PR then the machine could just be a scaled version of the same geometry.

Not only are there different types of compressor, they also vary in the number and complexity of the rows of blades depending on the size and thrust of the engine. The letter in Figure 1 indicates the type: F for fan, R for radial compressor and A for axial compressor. Fans move a lot of air but produce only a small pressure rise, so are close to the x-axis. Radial compressors move little air but can produce large pressure rises, so are close to the y-axis. Axial compressors are much more flexible, although they have other disadvantages. Depending on the number of stages, they are capable of a large range of pressure ratios over a large range of mass flows. They are scattered across the figure, although mainly on the diagonal. Thus, there is a large range of values covered in both dimensions by the different compressors.

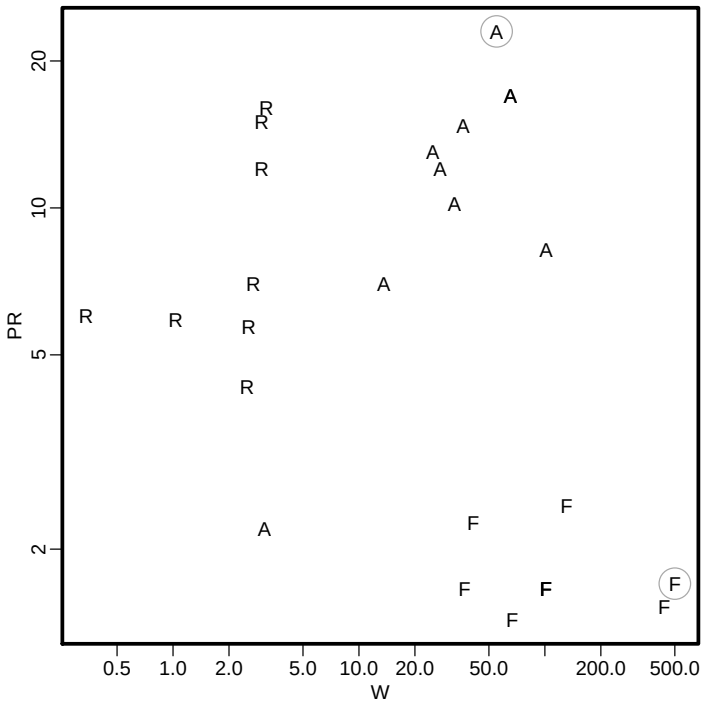

Figure 1. Compressor Design Points

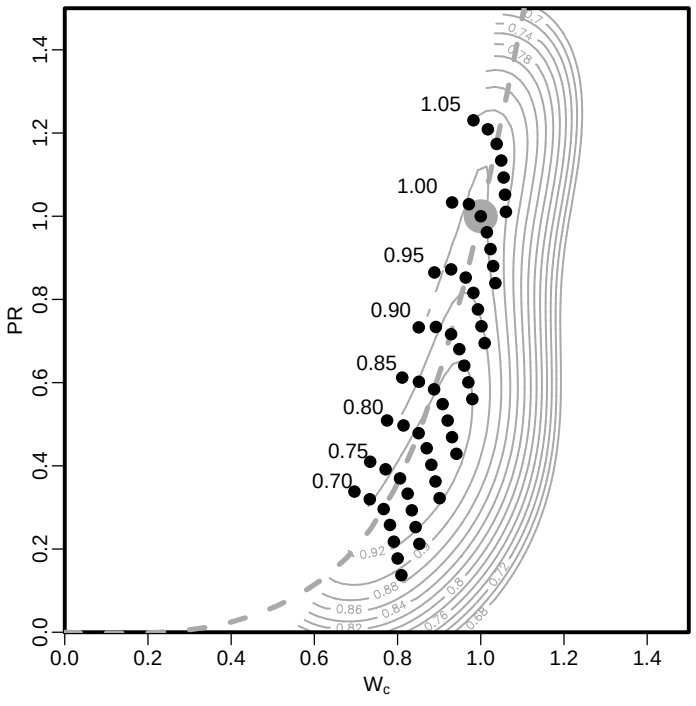

Figure 2. Fan

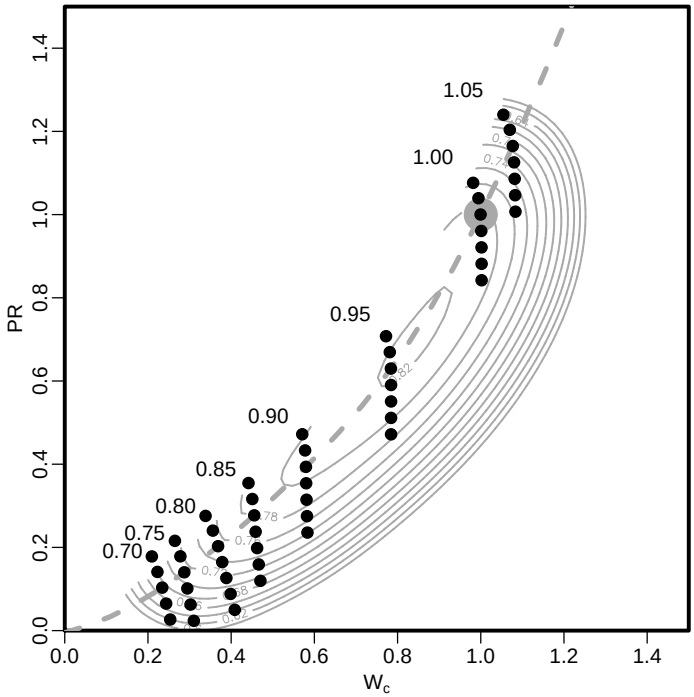

Figure 3. High Pressure Compressor

To get some idea of what this range means in terms of the shape of the maps, Figures 2 and 3 show two examples for two quite different compressors. Here, again the y-axis is the pressure ratio, but for off-design values for a single compressor. The x-axis is the mass flow, but now corrected for inlet temperature and pressure. In all our figures for compressor maps, pressure ratio and mass flow are relative to the design point i.e. $PR = (PR_{act} - 1)/(PR_{dp} - 1)$ and $W_c = W_{act}/W_{dp}$, respectively. Figure 2 is for a single stage fan [14], with a design point pressure ratio of 1.7 and mass flow of 500 kg/s. It is indicated by the F surrounded by a gray circle at the bottom right of Figure 1. Figure 3 is for a 10 stage high pressure compressor [8], with a design point pressure ratio of 23 and mass flow of 55 kg/s. It is indicated by the A surrounded by a gray circle at the top of Figure 1.

The black dots indicate speed lines. Each speed line captures the relationship between pressure ratio, mass flow and efficiency at a single compressor shaft speed. This is corrected for inlet temperature and normalized so that it is one at the design point. Both maps have speed lines for the same shaft speeds, the numbers are shown in the figures. The solid gray lines are contours giving the efficiency of the compressor. It is quickly apparent that there is much in common between the two maps, yet they are far from identical.

By using morphological image analysis techniques [3], we can extract the commonalities and differences in shape between compressor maps. The method relies on identifying common points on all shapes, called landmarks, and then finding the morphological operators needed to warp the points on one shape to those on another. Speed lines are a central feature of the compressor maps. In Kurzke and Riegler's [26] scaling procedure speed lines are not only changed in terms of mass flow, pressure ratio and efficiency but also given new speed values. Here, we compare maps by assuming speed lines of the same, normalized, value correspond on different maps. We believe this captures a very intuitive type of relationship between maps and one that exposes the important similarities and differences.

Following Kurzke and Riegler [26], a ridge, or backbone, is defined at the maximum efficiency point along these lines, indicated by the dashed gray line in Figures 2 and 3. Where the speed lines intersect with the ridge, an initial set of landmarks is defined. As speed lines do not have the same values for each map, we extract a consistent set of landmarks using interpolation, smoothing and extrapolation. We use a method based on domain knowledge to produce smooth but accurate new speed lines [27]. The system then places additional landmarks adjacent to the original set. These traverse along the speed lines at equal intervals, the black dots in the two figures. The size of the interval is determined by the curvature of the efficiency surface, normal to the ridge at the maximum efficiency point. Thus, maps that have sharper changes in efficiency, i.e. closer contours, have landmarks that are closer together.

For each map, there are eight sets of seven landmarks, most of them positioned below the ridge. Each set represents points on a single speed line. Two dimensional splines are used to interpolate and extrapolate efficiency values away from the landmarks. All the dimensions, except for efficiency, have been normalized such that the design point, indicated by the large gray dot, is one. By this means, we remove scaling information from the maps before extracting shape. Scaling information is still important but we consider it as a separate issue. As mentioned earlier, design of a new compressor often starts with an existing map that is simply scaled. So finding similar shaped maps with quite different design points would not be surprising.

2.2 The Relationship Between Maps

Figure 4 shows the effect of warping between the two compressor maps discussed in the previous section. The fan is at the bottom and the high pressure compressor at the top. As we move down the figure, starting with the high pressure compressor, several things happen. Firstly, the speed lines rotate and take on a more curved shape. Secondly, the efficiency increases. For each separate frame in the figure, the contours are at the same efficiency value. So, the increasingly wider space in the center of the contour lines, in the lower figures, indicates that the efficiency is rising. The three middle frames do not represent any of the 27 compressor maps discussed in the previous section. They have

been produced through the warping process. Yet, they certainly appear to be plausible maps, there is nothing counter-intuitive in their shapes. Many more new maps can be produced by warping between any two, or indeed several, existing maps.

To extract the commonalities between maps, this paper uses "relative warps" (an in-depth technical discussion can be found in [3]). A prototypical map is produced by averaging the (x,y,z) coordinates of each corresponding landmark (points on the speed lines) across all the maps. Warping this map will produce any other map. A thin plate spline defines the warp; it is easy to flex but bending it sharply is difficult. This encourages morphological operations that move the landmarks together in a smooth fashion. A thin plate spline basis function is used, $|X_i - X_j|$ the absolute distance between two points, for all three dimensions. The basis functions are located at each of the data points, the (x,y,z) coordinates of the landmarks of the prototypical map. Equation 1 shows the matrix form of this spline. X is a matrix of the data points, k is the number of landmarks, 1_k is a vector of ones, the elements of S are $s_{ij} = |X_i - X_j|$.

$$\begin{pmatrix} S+\lambda I & 1_k & X \\ 1_k^t & 0 & 0 \\ X^t & 0 & 0 \end{pmatrix} \tag{1}$$

Relative warps are defined using the "bending energy" matrix, which is sub-matrix $i, j = 1:k$ of the one produced by inverting the matrix in equation 1. Typically, in morphological analysis, solid body transforms are ignored, not being part of the shape of the objects. The solid body transforms are translation, scaling and rotation. As our z dimension is not normalized, we do not exclude these transformations, allowing the increase and decrease of efficiency to be modeled. The "bending energy" matrix is instead the sub-matrix $i = 1:k, j = 1:k+4$. Not being square, the Moore-Penrose [28] generalized inverse is used to invert this sub matrix. The weighting of the eigen values of this matrix encourages smooth warps. The resultant matrix, $B^-1/2$, is duplicated to form a larger matrix for all landmarks and all dimensions, shown in equation 2.

$$B_3^{-1/2} = \begin{pmatrix} B^{-1/2} & 0 & 0 \\ 0 & B^{-1/2} & 0 \\ 0 & 0 & B^{-1/2} \end{pmatrix} \tag{2}$$

2.3 Spectral Decomposition

The intent of the decomposition is to find a small set of dimensions that capture most of the variance between shapes. First a new matrix D in constructed by multiplying the covariance matrix C of the landmarks by the matrix of equation 2 and its transpose, as shown in equation 3.

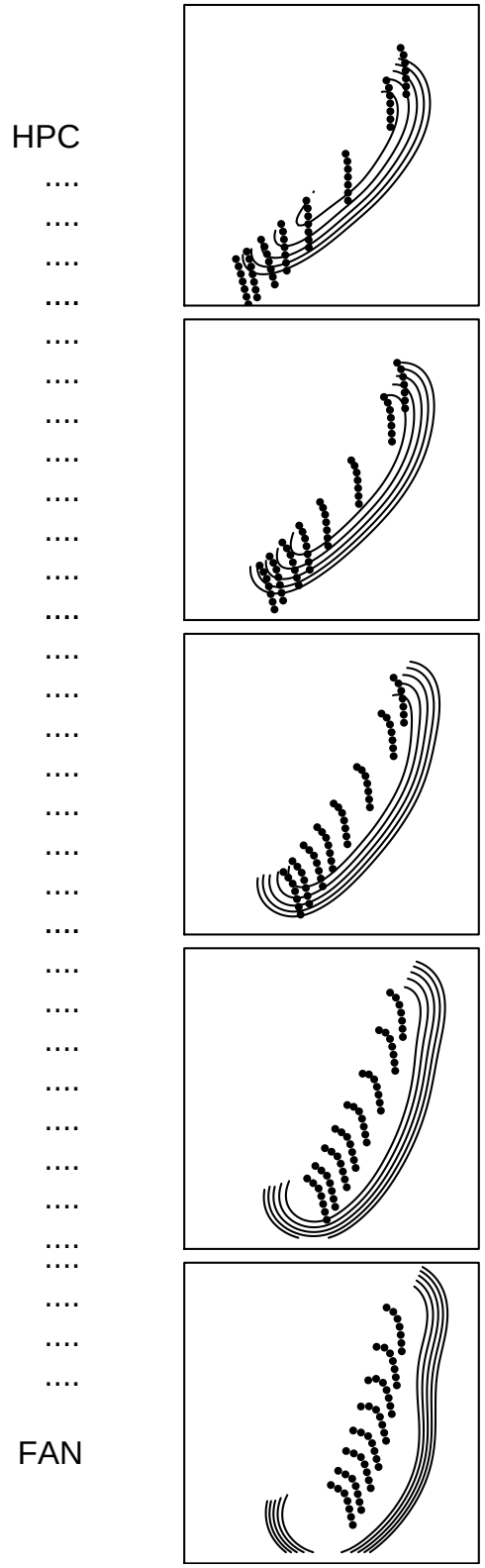

Figure 4. Warping between Maps

$$D = B_3^{1/2} C (B_3^{1/2})^t \tag{3}$$

The matrix D captures the differences between the position of landmarks across all the maps but with preference to those that involve smooth transformations. By then carrying a spectral decomposition of D, using singular value decomposition, we can identify the most important dimensions of change between maps.

$$U \Sigma V = D \tag{4}$$

The singular value vectors U of equation 4 describe different components of the warps between all the maps, essentially morphological operators. Each map can now be described in terms of these warps, which define the dimensions of our shape space. We can move back and forth between spaces using equations 5 and 6, where $(s_1, s_2, \ldots, s_n)_i$ are coordinates of map$_i$ in shape space and subscript p is the prototypical map.

$$(s_1, s_2, \ldots, s_n)_i = V B_3^{-1/2} ((x,y,z)_i - (x,y,z)_p) \tag{5}$$

$$(x,y,z)_i = B_3^{1/2} U (s_1, s_2, \ldots, s_n)_i + (x,y,z)_p \tag{6}$$

The end result of this process is to be able to smoothly warp from one map to another. This is achieved by a linear combination of map coordinates in the shape space. Each stage of the warp produces a new set of coordinates capturing the shape of a new map. Converting to the standard map space, using equation 6, produces a new set of landmarks. Fitting a curve through these landmarks results in a set of speed lines. Fitting a two dimensional spline to their efficiency values produces an efficiency surface. Together these define a new map. Most of the difference between maps is captured in the first two of these coordinates. We can study the effect of warping the prototypical map using only these two dimensions.

3 Analyzing the Maps

In this section, we use the mathematical apparatus introduced in the previous sections, particularly the spectral decomposition, to analyze how the shape varies across all types of map, as well as within each type. We present figures that capture both typical maps of the different types and the significant dimensions of variation. We discuss how these dimensions are tied to physical processes within the compressors. We also look at how the maps are grouped together based on these shape dimensions. We then illustrate how this approach can used to scale maps.

3.1 The Shape Variation

Figures 5, 6, 7, and 8 are for different sets of compressors: the complete set, just the fans, just the axial compressors, and just the radial compressors. Each figure forms a column containing three frames. At the top is a representative map, the prototypical map discussed in the previous section. The dashed lines are contours for isentropic efficiencies of 0.6 and 0.7. The figures also show points for the landmarks, on speed lines with values from 0.7 to 1 in 0.1 steps, all straddling a line representing the backbone. This is followed by the two most significant dimensions of shape variation between that set of maps. Each dimension includes the percent of variance it explains. So, in all cases about two thirds of the shape variation is accounted for in the first two dimensions. The light and dark shades of gray show the result of warping the representative shape, at the top, in the positive and negative directions, respectively, of that dimension. The black solid line is the backbone from the representative map at the top. The black arrows indicate how the lowest speed line would move when warped along this dimension.

The figures have been placed side-by-side for easy comparison, but let us for the moment concentrate on Figure 5 which analyzes the effect for all compressors. The major dimension of change shows that the speed lines range from well spread out, with a backbone that is slightly curved (the light gray), to much closer towards the top right hand corner, with a backbone that is strongly curved. The efficiency is increasing as we move from light to dark gray. What is additionally apparent in Figure 5 is that the speed lines range from close to vertical to close to horizontal. The second dimension shows a further movement of the speed lines down and to the right, but with no change in separation. This is accompanied by a commensurate shift in the position of the efficiency contours.

The very large changes in this data set are of no surprise as Figure 5 captures differences over a wide range of compressors. These go from very large, low pressure ratio, high mass flow, axial fans to small, high pressure ratio, radial compressors. Although the physical dimensions were not available for all the compressors, the maximum and minimum diameters, for those available are given in Table 1. The maximum and minimum of design pressure ratio and number of stages are also provided.

The rotation of the speed lines is likely due to differences between axial and radial compressors. Radial compressors are known to have a wider range of operation at a given speed. The close to vertical lines indicate choking, limiting the compressors operating range. The change in efficiency is partly due to the range of machines included in this study. A 1950's vintage compressor based on NACA blades will have a lower efficiency than a modern computer designed compressor. Another source of variation in efficiency is the large range of pressure ratios. Table 1 lists the relative pressure ratios. The highest is 51 times that of the lowest and efficiency is directly related to the pressure ratio. As we have normalized the dimensions in our figures, the pressure

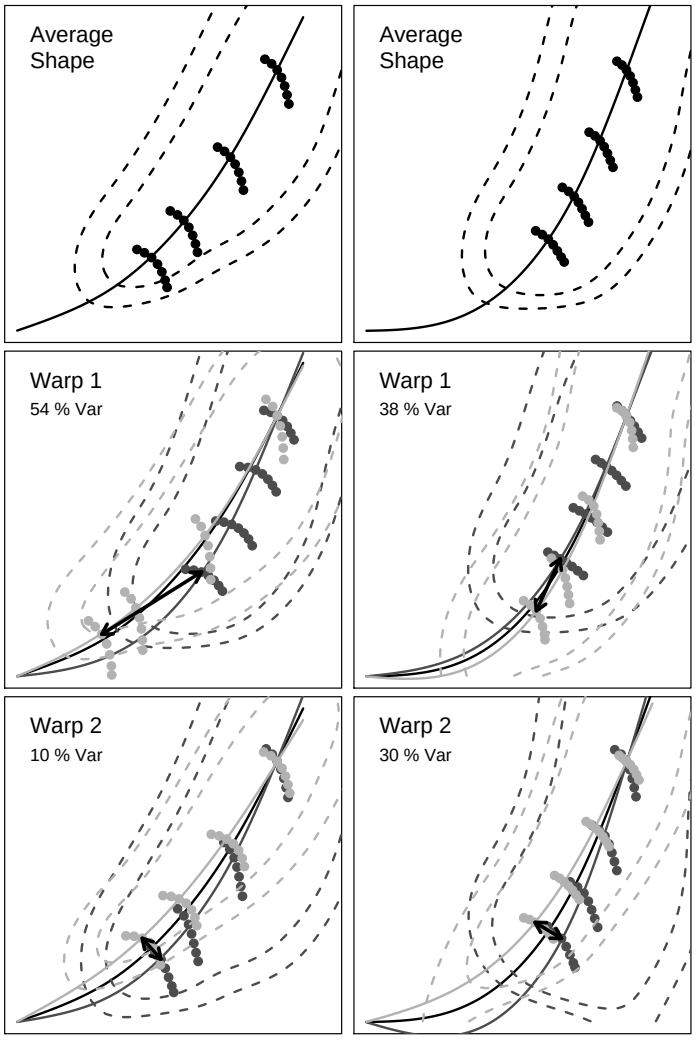

Figure 5. Warps: All Comps

Figure 6. Warps: Fans

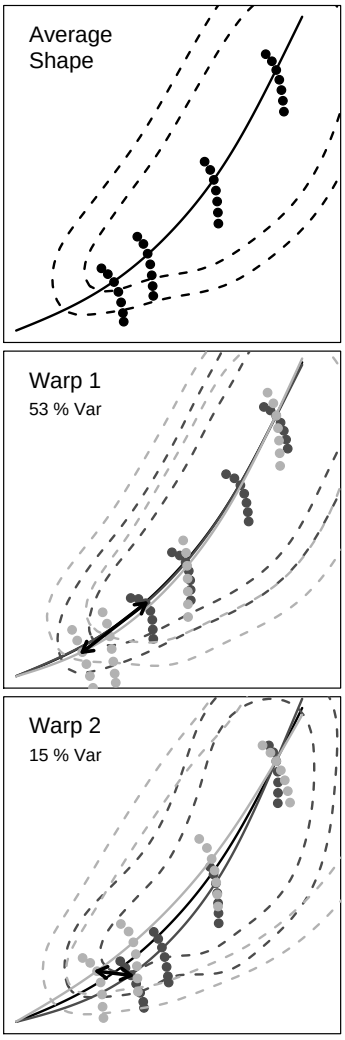

Figure 7. Warps: Axial

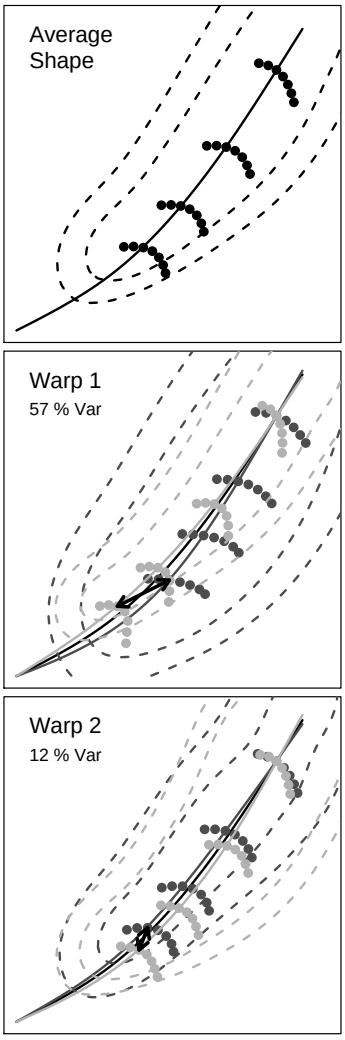

Figure 8. Warps: Radial

ratio on the y-axis is relative to that at the design point. However, the isentropic efficiency is dependent on the actual pressure ratio. For the same polytropic, or small stage, efficiency of 71% a fan with a $PR = 1.43$ would have a isentropic efficiency of 70% and an axial compressor with $PR = 23$ would have an isentropic efficiency of just 58%.

Figure 6, for the fans, shows a significant reduction in the range of mass flow for a fixed speed line, with the related change from horizontal to the choked vertical. This may be because compressor maps represent the aerothermal interactions in the machine, but the determining factor for a large fan design point is likely to be the mechanical stresses in the root of the blades. A large fan may never rotate fast enough to move the choked flow to the inlet, leaving the fan to operate in the more horizontal region of the speed lines. As the root stress is related to both the rotational speed and diameter, a smaller fan will be able to operate at a higher speed and approach closer to choked inlet flow.

The change in curvature of the backbone is a much larger factor for the fans, as is apparent in Figure 6. This may in part be related to the definition of the design speed. If the design speed is driven by mechanical considerations, it may actually deserve a lower value when compared to a high pressure compressor. This would push the speed lines down and change the shape of the backbone as they enter the more curved lower left section of the map. This is further reinforced by the change in efficiency contours which, although show some change in absolute levels, show a significant shift in position for the second warp.

The axial compressors in Figure 7, however, appear to have much more consistent design speeds. The backbones and design speed lines are almost coincident through both warps. The first warp has very little affect on the position of the efficiency contours and the second very little effect on that of the speed lines.

Type	PR			Diameter (m)			Stages	
	max	min	$\frac{max-1}{min-1}$	max	min	$\frac{max}{min}$	max	min
All	23	1.43	51	1.86	0.102	18.3	17	1
Fans	2.45	1.43	3.4	1.86	0.508	3.67	1	1
Axial	23	3.1	11	1.14	0.491	2.33	17	2
Radial	15	4.3	4.2	0.290	0.102	2.85	2	1

Table 1. Pressure ratios and diameters for each compressor class

Although the efficiency change is partly due to compressor design it is also strongly affected by the pressure ratio, which has the largest range of the three sets of machines. The first warp, interestingly, moves the 0.9 speed line to become coincident with the 0.8 speed line at the other end of the warp. It is possible that speed lines have been mislabeled at some point in the reporting process.

We would, however, expect the speed lines to spread out further, with respect to pressure ratio, as the number of stages increases. For example, if a single stage compressor increases the pressure by 10%, 5 similar stages, in series, will raise the pressure by 61%. If we imagine an additional single stage increase of 10% this would result in a rise of 88% in the 5 stage system. The outcome being that if pressure ratio of a single stage was directly linked to speed, the single stage compressor would have speed lines equally spaced on the pressure ratio axis while the 5 stage would have increasingly larger gaps. Table 1 shows that the axial compressors have a very large range of stage numbers generating different speed line spacings.

The radial compressors, Figure 8, show a greater change in backbone than the axial ones but significantly less than the fans. We also see a change in shape of the speed lines similar to the fans, moving from nearly horizontal to extending into choke. This may be due to reasons similar to those hypothesized for the fans. The design speed may not have a consistent definition. As the design speed line rotates closer to choke, the choke point is being moved towards the inlet of the compressor. An alternative explanation is that a single compressor is causing a large portion of the change. The only radial compressor map sampled that did not extend the higher speed lines into choke was the calculated single stage compressor from NASA [10]. If a calculated map is significantly different from all the measured maps it leads to the conclusion that the calculation was lacking in some aspect and is incorrectly biasing the results. Removing this map from the radial compressor set has little effect on the backbone warp but significantly reduces the changes in speed line shape warp. The design speed lines become almost coincident in both the warp 1 and 2 plots.

3.2 Grouping the Compressors

Figure 9 shows the effect of clustering [1] based on the two dimensions for all compressor maps, shown in Figure 5. We fix the number of groups to three, as many as there are compressor types. This clustering finds the natural grouping of the points based solely on their values for the two shape dimensions. Thus, it should capture the common performance characteristics embodied in the maps. The three groups are represented by different symbols: diamonds, circles and squares. When we label the points according to the compressor type, the symbols and labels largely agree. In fact, the first dimension alone captures much of the difference. Going from left to right there are fans, radial compressors and axial compressors. This is in part due to the pressure ratio generated by each machine as there is a good correlation between the warp 1 values and pressure ratio. More weakly, the types also seem to be differentiated on the warp 2 value. For the most part the radial compressors are above the axial compressors and fans.

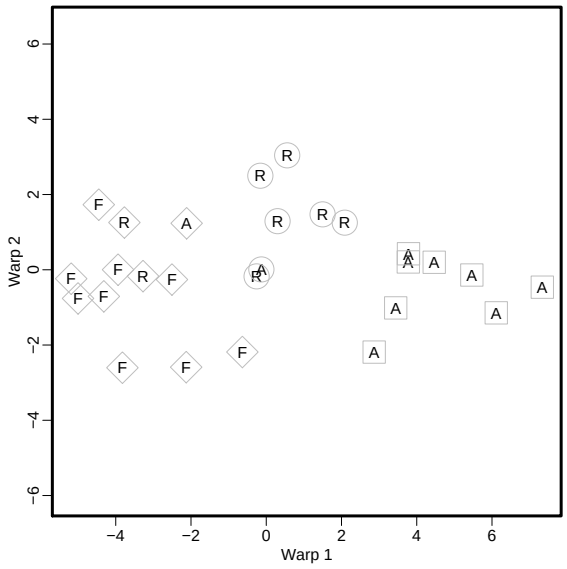

Figure 9. Clustering on the First Two Warps

There are however a few exceptions, where one type of compressor seems much closer to another type than its own. Figure 10 shows the clustering of axial compressors alone. The compressor indicated by the dark gray circle has only two stages. It therefore has properties more like a fan than a many staged high pressure compressor. It is placed close to the fan cluster in Figure 9, the A in the diamond shape. The compressor indicated by the dark gray circle is also outside the cluster of the other axial compressors, closer to the radial compressors in Figure 9, the A

[1] k-means clustering is used.

in the circle in the middle of the figure. This compressor is differentiated by its old technology. It is a 1950's vintage compressor and would be significantly different from the other compressors which date from the late 1970's to early 1990's.

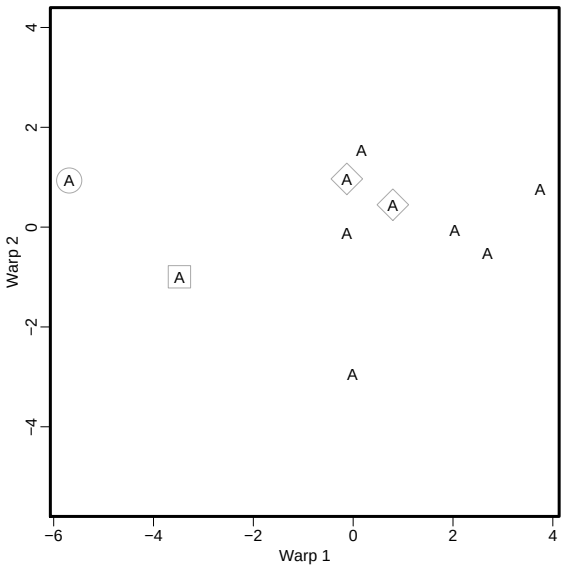

Figure 10. Clustering the Axial Compressors

It is interesting to compare the two compressors indicated by the dark gray diamonds in Figure 10. They are almost identical in the second dimension and very close in the first. They should, however, be coincident as they are actually the same compressor. One was taken from Stevenson and Saravanamuttoo [23] who reference Klapproth et al. [17], the source of the other. Although, it is reassuring that the two maps are clustered close together in Figure 10, the difference indicates that errors can be introduced by the reporting and transcribing of the data.

The three points in Figure 11 indicated by the gray circles are for the same compressor with different inlet guide vane angles (0, 20, 40 degrees). They are all calculated with a NASA program from 1984 [10]. The similarity of the compressors is shown by the cluster with a distinct progression from lower left to upper right. The compressor, indicated by the gray square is also produced with the same family of NASA code. The first dimension for this family of compressors is correlated to the pressure ratio. If we normalize both the warp and the pressure ratio we find a very strong linear correspondence. Unfortunately the high percentage of calculated maps in the fan data set (44%) makes finding correlations problematic. We may be finding factors that are more to do with the map calculating software rather than true physical relations. For the purposes of generating warps, in the future we may limit the influence of calculated maps. We would

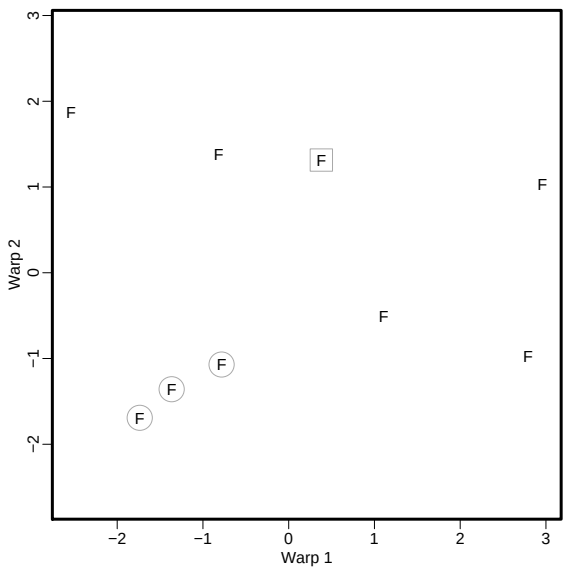

Figure 11. Clustering the Fans

be reluctant to remove them entirely as they represent useful expert opinion realized in the map generator.

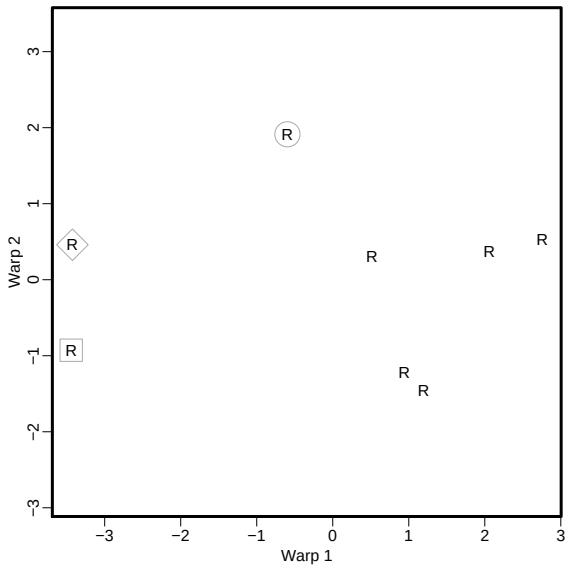

Figure 12. Clustering the Radial Compressors

The radial compressors in Figure 12 show the gray circle outside the main cluster. This compressor [22] included a passive inducer shroud bleed to increase surge margin and it had a high blade count and strongly backswept blades, which we would expect to differentiate it from a standard radial compressor. The

gray diamond compressor [20] had an even higher blade count and also incorporated more modern design techniques. It resulted in a much larger, nearly horizontal, section for each speed line than is typical. This may explain the proximity in the first dimension to the gray square [10] since it also had a very large horizontal section and included very little or none of the choked section of the line. As this was only a calculated map code may not have captured the entire or true performance a compressor.

3.3 Using the Warps for Scaling

Not only do the warps expose interesting similarities and differences across compressors, they can also be used to produce a new map. We begin by locating maps that are close in some sense to the target map. As in Kurzke and Riegler's work [26], we use design pressure ratio and mass flow to identify candidate maps for scaling. From section 3.1, we know that these values are at least weakly correlated to the shape dimensions. Unlike previous work, the "scaled" map is actually the average of three maps. To identify these maps, we first find the one whose design point is closest to the target value. The two other maps chosen enclose the target design point within a triangle. We then average the shape coordinates of the three maps, weighted by their closeness to the target design point. The new set of coordinates is converted back into map space producing a new map.

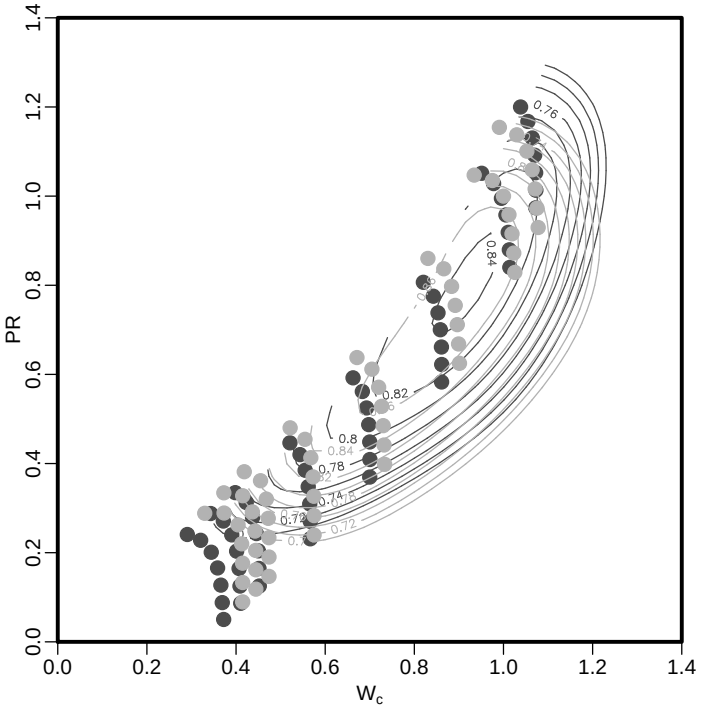

Figure 13. Producing a new Map

An example, a high pressure compressor, is shown in Figure 13. In general the new map, indicated by the light gray, is in good agreement with the target map, indicated by the dark gray. There is some difference in the position of the speed lines, particularly as one moves away from the design point. Earlier experiments [29] suggest that this is generally an accurate method of producing new maps. As the design pressure ratio and mass flow are only weakly correlated with shape, other information should make selection of candidate maps better and thus produce a more accurate new map. What we have achieved here is to effectively model the performance of existing compressor even though we did not have the original map.

4 Limitations and Future Work

At present, the scaling uses warps derived from all compressors. This reduces the need for extrapolation when the new design point is outside the range of one compressor type. In future, the warps will be generated dynamically based more closely on similar compressors. This should produce more accurate scaling. As the shape of the new maps is determined by the warps, this gives some support, along with the clustering discussed in the previous section, that the warps capture important properties. In the future, we aim to include the surge margin. At present, however, there is a question of the validity of the surge line on some of the maps. Although most of the maps produced by scaling are totally plausible, it may still occur, especially when extrapolating, that physically impossible maps result. Our aim is to introduce further constraints to limit this possibility.

5 Conclusions

In this paper, we have stressed the importance of the production of accurate compressor maps. We have presented a way of analyzing the commonalities and differences in shape for a large range of maps of different types. Not only was the total shape change determined, but also the principal dimensions of that change. We presented figures for both typical maps of various types and the significant dimensions of variation between types. We discussed how these are tied to physical processes within the compressors. We hope that this has given insight into how the shape of a map depends on the compressor type and design point characteristics. We believe this insight should accelerate map construction. We also illustrated how the method can be used directly in the production of new maps.

Acknowledgments

We would like to thank our colleagues in the Institute of Information Technology and in the Institute of Aerospace Research for many useful discussions and suggestions. We particularly thank Jeff Bird, Sylvain Létourneau and Chusheng Yang.

REFERENCES

[1] Visser, W., and Broomhead, M., 2000. "GSP, a generic object-oriented gas turbine simulation environment". In Proc. of ASME Gas Turbo Expo, 2000-GT-0002, pp. 8–11.

[2] Sellers, J. F., and Daniele, C. J., 1975. DYNGEN-A program for calculating steady-state and transient performance of turbojet and turbofan engines. Tech. Rep. NASA-TN D-7901.

[3] Dryden, I., and Mardia, K., 1998. *Statistical Shape Analysis*. John Wiley and Sons, Chichester, UK.

[4] Ball, C., 1989. Advanced technologies impact on compressor design and development: A perspective. Tech. Rep. NASA-TM-102341.

[5] Belaygue, P., and Vignau, H., 1987. "Le compresseur centrifuge, cornposant essentiel des turbomoteurs de petite et moyenne puissance". In Proc. of Symposium on Technology Requirements for Small Gas Turbines, AGARD-CP-537, pp. 15–1 to 15–15.

[6] Boyd, D., 1987. "Development of a new technology small fan jet engine". *Canadian Aeronautics and Space Journal,* **33**(2), pp. 84–90.

[7] Carchedi, F., and Wood, G., 1983. "Design and development of a 12:1 pressure ratio compressor for the ruston 6-mw gas turbine". In Proc. of 28th ASME International Gas Turbine Conference, 82-GT-20.

[8] Cline, S., Fesler, W., Liu, H., Lovell, R., and Shaffer, S., 1983. High pressure compressor component performance report. Tech. Rep. NASA CR-168245.

[9] Colantuoni, S., and Liotti, G., 1987. "Experimental investigation on small turboprop behaviour under compressor rotating stall for different inlet flow conditions". In Proc. of Symposium on Engine Response to Distorted Inflow Conditions, AGARD-CP-400, pp. 14–1 to 14–16.

[10] Converse, G., 1984. Extended parametric representation of compressor fans and turbines vol. iii - modfan user's manual (parametric modulating flow fan). Tech. Rep. NASA CR-174647.

[11] Converse, G., 1984. Extended parametric representation of compressor fans and turbines vol. i - cmgen user's manual. Tech. Rep. NASA CR-174645, Washington, D.C.

[12] Cornell, W., 1975. Health experimental quite engine program - summary report. Tech. Rep. NASA CR-2519.

[13] Creason, T., and Baghdadi, S., 1988. "Design and test of a low aspect ratio fan stage". In Proceeddings of 24th AIAA Joint Propulsion Conference, AIAA-88-2816.

[14] Freeman, C., and Cumpsty, N., 1992. "Method for the prediction of supersonic compressor blade performance". *Journal of Propulsion,* **8**(1), pp. 199–208.

[15] Geiselhart, K.A.; Caddy, M., and Morris, S. J., 1991. Computer program for estimating performance of air-breathing aircraft engines. Tech. Rep. NASA TM-4254.

[16] Kashiwabara, Y.and Katoh, Y., Ishii, H., Hattori, T., Sasada, T., and Matsuura, Y., 1990. "Developments leading to an axial flow compressor for a 25mw class high efficiency gas turbine". In Proc. of ASME Turbo Expo, 90-GT-238.

[17] Klapproth, J., Miller, M., and Parker, D., 1979. "Aerodynamic development and performance of cf6-6/lm2500 compressor"". In Proc. of 4th International Symposium on Air Breathing Engines, AIAA-1979-7030, pp. 243–249.

[18] Klassen, H.A.; Wood, J., and Schumann, L., 1977. Experimental performance of a16.10-centimeter-tip-diameter sweptback centrifugal compressor designed for a 6:1 pressure ratio,. Tech. Rep. NASA T M X-3552.

[19] Kong, C., Ki, J., and Kang, M., 2003. "A new scaling method for component maps of gas turbine using system identification". *Journal of Engineering for Gas Turbines and Power,* **125**(4), pp. 979–985.

[20] Krain, H., Hoffmann, B., and Pak, H., 1995. "Aerodynamics of a centrifugal compressor impeller with transonic inlet conditions". In Proc. of International Gas Turbine and Aeroengine Congress and Exposition, 95-GT-79.

[21] Love, C., 1987. "Design and development of an advanced f100 compressor". In Propulsion and Energetics Panel 69th Symposium, AGARD-CP-421, pp. 36–1 to 36–12.

[22] Palmer, D., and Waterman, W., 1994. "Design and development of an advanced two-stage centrifugal compressor design and development of an advanced two-stage centrifugal compressor". In Proc. of Turbo Expo, 94-GT-202.

[23] Stevenson, J., and Saravanamuttoo, H., 1995. "Simulating indirect thrust measurement methods for high-bypass turbofans". *Journal of Engineering for Gas Turbines and Power,* **117**, pp. 38–46.

[24] Tesch, W., and Pase, R., 1983. "Design and performance of a low aspect ratio, high tip speed, multi-stage axial compressor". In Proc. of Nineteenth AIAA Joint Propulsion Conference, AIAA-83-1161.

[25] Yoshinaka, I; Thomson, R., and Letourneau, J., 1989. "The performance prediction and demonstration of a centrifugal compressor for the multiple purpose small power unit". In Proc. of International Turbo Expo, 89-GT-112.

[26] Kurzke, J., and Riegler, C., 2000. "A new compressor map scaling procedure for preliminary conceptional design of gas turbines". In Proc. of ASME Turbo Expo, 2000-GT-0006.

[27] Drummond, C., and Davison, C., 2009. "Improved compressor maps using approximate solutions to the moore greitzer model". In Proc. of ASME Turbo Expo, GT2009-60148.

[28] Larson, R., Edwards, B. H., and Falvo, D. C., 1996. *Elementary Linear Algebra*. Houghton Mifflin Co.

[29] Drummond, C., 2007. "Learning multi-dimensional functions: Gas turbine engine modeling". In Proc. of 11th European Conference on the Principles and Practice of Knowledge Discovery in Databases, LNAI 4702, pp. 406–413.